PAPER

Experimental decay-heat simulation-benchmark for 14 MeV neutrons & complex inventory analysis with FISPACT-II

IOP Publishing | International Atomic Energy Agency Nuclear Fusion

Nucl. Fusion **59** (2019) 086045 (16pp) https://doi.org/10.1088/1741-4326/ab278a

Experimental decay-heat simulation-benchmark for 14 MeV neutrons & complex inventory analysis with FISPACT-II

M.R. Gilbert[1] **and J.-Ch. Sublet**[1,2]

[1] Culham Centre for Fusion Energy, United Kingdom Atomic Energy Authority, Culham Science Centre, Abingdon, OX14 3DB, United Kingdom of Great Britain and Northern Ireland
[2] Nuclear Data Section, International Atomic Energy Agency, PO Box 100, 1400 Vienna, Austria

E-mail: mark.gilbert@ukaea.uk

Received 5 March 2019, revised 9 May 2019
Accepted for publication 6 June 2019
Published 5 July 2019

Abstract

Nuclear inventory simulations have a vital role to play in the planning and execution of future fusion experiments and power plants. They are able to predict the transmutation (burn-up) response of material compositions under neutron irradiation, thus providing information about the build-up of impurities that could impact on material performance. The inventory evolution also quantifies the radiological response of a material by tracing the production (and decay) rates of radioactive nuclides. This information can be used to plan maintenance schedules at nuclear facilities, satisfy nuclear regulators during reactor planning, and quantify the waste disposal needs during reactor decommissioning.

However, the validity of inventory simulations must be verified to give confidence in the predictions. This paper describes a validation and verification (V&V) benchmark exercise that tests the quality of nuclear code predictions. Such benchmarks are an important part of the development and release of the FISPACT-II inventory code and its associated input nuclear data libraries. This paper describes the latest V&V based on the fusion decay-heat measurements performed at the Japanese FNS facility. Rigorous and detailed assessment techniques, focussed on the complex breakdown of decay-heat contributions from individual radionuclides, have been employed to interpret the simulated results, benchmark the data against the experimental measurements, and to compare results from different international nuclear data libraries. Example results are presented and discussed for nickel, iron, niobium, tungsten, chromium, and osmium, using FISPACT-II simulations performed with TENDL-2017, JEFF-3.3, ENDF/B-VIII.0, EAF2010, and IRDFF-1.05 nuclear cross section libraries.

Keywords: fusion decay-heat measurements and simulation, nickel and iron, tungsten and osmium, chromium, niobium, nuclear data validation, nuclear reactions and isomeric states

(Some figures may appear in colour only in the online journal)

1. Introduction

In nuclear fusion energy research (magnetic-confinement or otherwise) many of the outstanding technical issues that must be solved in a successful demonstration of fusion's viability as a commercial energy source relate to the choice and configuration of materials within the reactor. There is significant research and discussion in the selection process of materials (see, e.g. [1–3]). How a material will perform structurally or functionally under the extremely challenging environment associated with the high energy neutrons emitted from the fusion plasma is a major concern for plant reliability and availability, and will necessarily influence many of the reactor design choices for a future demonstration fusion power plant (often called

'DEMO') [3]. Current estimates of material exposure conditions for in-vessel components in DEMO indicate tens of dpa (displacements per atom) during a lifetime (see [3, table 3]) and heat loads of 10–20 MW m^{-2} in some plasma-facing materials [4]. Besides this physical material damage, reactor operation (and decommissioning) must also be concerned with the transmutation aspect of nuclear interactions because the change in isotopic/elemental/chemical compositions can also influence material behaviour and performance as well as produce radioactive components. The radioactivity, in particular, will constrain in time and cost the (remote) maintenance options during operation, as well as determining the economic and environmental cost of waste disposal [5, 6]. Similar concerns will also influence design choices for the next generation (IV) of fission plants, where the energies and fluxes of neutrons are higher than in earlier generations. Accurate knowledge of the expected changes to materials under neutron irradiation is clearly a vital ingredient in nuclear (fusion or fission) power-plant planning. In the absence of experimental facilities at the relevant energies and fluxes expected in a power plant, assessment of isotope composition evolution, and hence the consequences for material behaviour and activation, must rely on predictions from simulations [7].

Modelling how the isotopic composition (the 'inventory') of a material evolves in-time under neutron irradiation is often accomplished using inventory simulation codes. Such codes take a specified neutron flux-energy distribution as input, most often (for conceptual reactor designs) calculated using Monte-Carlo statistical neutron transport simulations, and solve a set of coupled, stiff, ordinary differential equations that relate the rate-of-change of concentration N_i of each nuclide i to the (total) reaction cross sections that either destroy or create it, viz:

$$\frac{\mathrm{d}N_i}{\mathrm{d}t} = \underbrace{-N_i(\lambda_i + \sigma_i\phi)}_{\text{destruction}} + \sum_{j\neq i} \underbrace{N_j(\lambda_{ji} + \sigma_{ji}\phi)}_{\text{creation}}, \tag{1}$$

where λ_i is the decay constant (in s^{-1} units) for nuclide i and σ_i in barns is the total cross section summed over all reactions that destroy it, which is typically evaluated by folding (vector dot product) the normalized input neutron flux spectrum with energy-dependent reaction cross sections in the same energy-group format read from a specified library database. ϕ is the total neutron flux in n cm^{-2} s^{-1}, and the product $\sigma\phi$ is a per second reaction rate. λ_{ji} and σ_{ji} are the equivalent total decay constants and total cross sections on all other nuclides j that create i. It is assumed that the (neutron) particle flux ϕ is not significantly modified by the changing material composition [8], which is valid in most situations apart from very high burn-up (transmutation) scenarios (e.g. in fission fuels or in lithium-based tritium breeder blankets for fusion) where alternatively the neutron flux spectrum can be periodically updated in an inventory-code-to-transport-code loop (see, for example, [9, 10]). With the constant flux assumption (i.e. for a small enough time interval Δt) the rate equations remain linear (in time) and the decay constants and cross sections in equation (1) are independent of N values, resulting in the matrix form

$$\frac{\mathrm{d}\mathbf{N}}{\mathrm{d}t} = \mathbf{A}\mathbf{N} = (\mathbf{\Lambda} + \phi\mathbf{\Sigma})\mathbf{N}, \tag{2}$$

where the independent matrix $\mathbf{A}$ (and its decay rate $\mathbf{\Lambda}$ and cross section $\mathbf{\Sigma}$ sub-matrices) are assembled from the components of equation (1) [8].

A world-leading platform for predicting inventory evolution is the FISPACT-II [8, 11, 12] code. Building on several decades of development, FISPACT-II has been re-engineered and modernised to take advantage of the latest international nuclear data libraries, which it uses to construct the matrix $\mathbf{A}$ in equation (2). This matrix is sparse, containing only around 0.8% non-zero elements in a non-fission scenario [8], because each reaction/decay typically produces single daughter nuclides (and secondary products). It is also stiff due to the many orders of magnitude variation in decay rates that produce large fluctuations and numerical instability. FISPACT-II uses the well-established LSODE [13, 14] package to solve such linear, stiff and sparse systems and hence evolve nuclide compositions in time.

The FISPACT-II code methodology has been thoroughly tested for robustness but the accuracy and reliability of its predictions are only as good as the nuclear data fed into it. Validation and verification (V&V) benchmark exercises are needed to test both the performance of the code and the quality of the nuclear databases.

Several of these 'benchmarks' have been developed for neutron-irradiation applications with FISPACT-II, including an integro-differential validation [15], which compares, amongst other things, the available experimental differential data from the EXFOR [16] database to reaction cross section evaluations read from data-libraries by FISPACT-II. Ideally, all reaction cross sections at all neutron energies would be benchmarked in this way using differential data. However, it is expensive and difficult to produce such data, which typically comes from carefully performed measurements under near-monoenergetic neutron fluxes that can be directly converted into a reaction cross section at a single (neutron) energy. Thus, differential experimental data only covers a small fraction of the total number of important nuclear reactions, and even for reactions with differential data, the neutron-energy coverage is usually incomplete [17, 18].

'Integral' measurements, on the other hand, can often be relatively inexpensive and more-straightforward to obtain. Usually produced from an experiment where materials are exposed to a complex energy-flux spectrum of incident neutrons, integral data is difficult to attribute to a single reaction channel and it is virtually impossible to use it to reconstruct the energy-dependent reaction (probability) cross sections. This makes the interpretation of such experiments more difficult and forces their use in a complete simulation benchmark—one where the experimental procedure is faithfully modelled and the complete nuclide inventory evolution is simulated in time to output quantities that can be directly compared to the real measurements. Carefully constructed simulation benchmarks of this kind test both the inventory simulation tool—in the present work FISPACT-II—as well as the quality of the underlying nuclear data.

Integral benchmarks used in the V&V of FISPACT-II and neutron-reaction and nuclide-decay data include a fission decay-heat and inventory benchmark [19], which primarily tests fission yield and decay-heat data (as well as FISPACT-II's application of them) against fission decay-heat measurements, and the pseudo-differential benchmark of Maxwellian-averaged cross sections against high-energy, astrophysics data [20]. For nuclear fusion, we have also developed a largely automated decay-heat benchmark that compares simulated predictions to a database of integral experimental measurements obtained by the Japan Atomic Energy Agency (JAEA) at their fusion neutron source (FNS) facility.

This paper focuses on the fusion decay-heat benchmark, taking results from the latest technical report on the benchmark [21] with further analysis. The paper is organized as follows: we begin with a description of the FNS experimental set-up and measurements, before explaining the benchmark simulation process. The results section considers several important materials from the fusion perspective, revisiting the relevant output from the latest technical report on the benchmark [21] and expanding on the analysis and discussions therein. These examples highlight the complexity of the simulations necessary to replicate the superficially simple integral experiment; the total decay-heat maybe a single measure, but many contributing nuclear reactions and decay processes often have to be simulated to accurately predict it. The fact that these complex contributions are, in some cases, able to predict the experimental result to high accuracy is testament to the quality of modern nuclear data libraries and also demonstrates the efficacy of FISPACT-II's computational algorithms.

2. The FNS experiment

As well as the need to provide nuclear data to evaluators, the absence of experimental data on decay power output (i.e. decay-heat) was also a driving force behind the planning of a series of experiments at the FNS facility at the JAEA by Maekawa *et al* [22–26]. Accurate prediction of residual decay power is necessary to plan for off-load cooling requirements in nuclear power plants and to aid the design of mitigation steps for loss-of-coolant accident events. JAEA performed a series of experiments during the period 1996–2000 at the FNS facility. 73 different materials, consisting primarily of pure metals, alloys, and oxides, were irradiated for either 5 min or 7 h (or both) in a 14 MeV neutron source generated by a 2 mA deuteron beam impinging on a stationary tritium-bearing titanium target. The resulting neutron fluxes were typically around 1.0×10^{10} n cm^{-2} s^{-1}, which were calculated to within 5% accuracy using a high-purity germanium detector to measure the rate of the well-characterised ^{27}Al(n,α)^{24}Na reaction in aluminum reference foils attached to each sample [23]—a similar methodology has also been employed by the authors of the present work in γ-spectroscopy experiments [27, 28].

Thin material samples, 25×25 mm^2 in area, and around 10 μm thick, were used in the experiments, either as metallic foil or alloy/oxide powder sandwiched between tape. Use of a thin sample minimised the self-absorption of β-rays emitted in the sample itself and thus allowed the subsequent heat-output measurement to be as accurate and representative as possible.

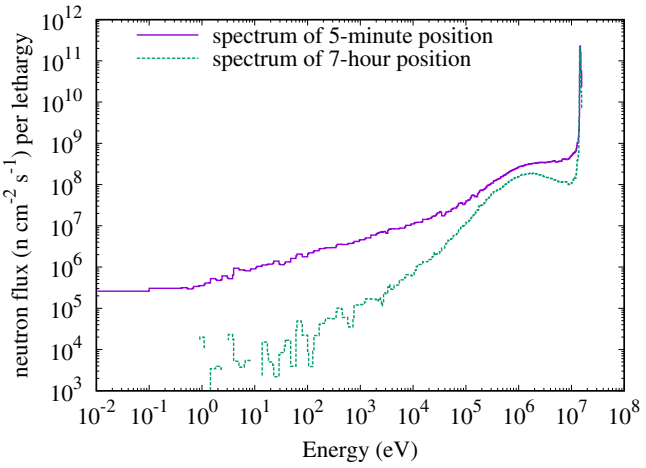

Figure 1. Simulated neutron spectra experienced by the two experimental batches performed at JAEA's FNS facility and discussed in this paper. Flux values are scaled (divided) by lethargy to remove weighting bias caused by the varying energy-bin widths. Lethargy is the natural log of the ratio of an energy bin's upper and lower bounds.

After exposure, each sample was extracted to a whole energy absorption spectrometer (WEAS) where the decay-heat (converted from the pulse height spectra recorded by the WEAS) was measured at various time intervals as the material decay-cooled. A pneumatic tube or 'rabbit' was used to extract the samples after the short, 5 min irradiations, allowing the first decay-heat measurements to be recorded within the first minute of cooling [22]. The WEAS system, which comprised of two large bismuth-germanate BGO scintillators in a geometric arrangement, provided almost 100% detection efficiency for both β and γ-rays.

Over the course of the experimental series, samples were irradiated at different positions within the facility as the orientation of the tritium target, deuteron beam, and sample varied according to the needs of the experiment (in particular due to the positioning of the fast extraction 'rabbit' system for the 5 min experiments). This variation lead to results produced in several batches. The full report [21] benchmarks against all of this data, but in the present paper we focus on the final batch (in 2000) of 5 min experiments performed for all 73 different material-types at an irradiation position where the pneumatic tube was parallel to the deuteron beam and the samples sat around 50 mm from the tritium target (position 1 described in [21, 26])—a specially commissioned batch not discussed in the JAEA reports [24–26]. For the 7 h irradiations, a subset of the full material list were irradiated without the pneumatic tube (rapid extraction was not needed as the first measurement was typically performed about 16 h after the irradiation in those cases) and with the samples sat almost directly on the tritium target, with only a cooling water channel in between (position '7' in [21, 26]).

The neutron spectrum at each irradiation position was calculated using the Monte-Carlo code MCNP [29], and figure 1 shows the spectra for the experimental positions of the two

batches considered in this paper. The neutron flux profiles indicate a marked 14 MeV fusion peak and very few neutrons at energies lower than 1 MeV. The typical uncertainty at energies below 100 eV was large (Maekawa *et al* estimated a 20% experimental uncertainty in the decay-heat when dominated by capture reactions involving a majority of lower-energy neutrons [26]) and so few reaction rates can be well characterised at these energies. If lower energy neutrons are important for a production pathway of a simulated radionuclide, the comparison to, and validation against, the experiment will not be fully valid.

Despite the foregoing, Maekawa *et al* were confident enough in their experimental procedure to quote the measured decay-heat values with errors in the range 6%–10% in most cases, which included errors associated with the neutron flux determination (from the Al reference foils), in the WEAS energy calibration, and in the correction factors applied to account for the efficiency limits of the WEAS [22, 26].

3. Simulation and analysis methodology

The reported data for the experiments were very detailed, with, in particular, very precise measurement times, which has allowed the design of simulations to replicate the experiment in a very robust and accurate manner. For each case, a FISPACT-II [11, 12] simulation (or simulations if several different nuclear databases are being tested) was performed using all the experimental parameters. These included the starting material composition as assumed and quoted by JAEA—Maekawa *et al* [22] noted that there were additional unknown errors associated with uncertain impurities in the chemical compositions of some samples, which in the present work, for example, is seen to impact the analysis of the chromium experiments (section 4.5). As well as the irradiation times (5 min or 7 h), the experimental record also included unique, sample-specific cooling times between the decay-heat measurements in the WEAS.

In the latest application of the decay-heat benchmark [21], separate FISPACT-II simulations were performed with the current releases of major international nuclear cross section libraries (and their associated decay-data files where appropriate). TENDL-2017 [30], ENDF/B-VIII.0 [31], and JEFF-3.3 [32] were considered alongside the older EAF2010 [33] library, which is still widely used in the fusion research community in Europe. Additionally, the 79 dosimetry reactions [34] of IRDFF-1.05 [35] were also accessed (FISPACT-II is uniquely capable of utilising any appropriately formatted data library—even one with a small list of defined target nuclides and possible reactions), but simulations with that (deliberately) limited database are only meaningful for certain samples.

The FISPACT-II simulation results have been compared to the corresponding experimental data via a set of automated analyses and visual representations that have been developed over a number of years. These allow not only the comparison between the simulated total decay-heat and the experimental measurements, but also probe in-depth the underlying complexity of the inventory evolution, including the time-varying relative importance of decay-heat from different radionuclides, their uncertainties, and their reaction pathways of production—all of which is part of the standard capabilities of FISPACT-II. In the benchmark reports [21], results and comparisons are presented for each sample experiment in both graphical and tabulated form, and some simple analyses are performed to assess the quality of code predictions, including standard experiment to calculation ratios, commonly known as C/E values. Work is ongoing to consider more advanced statistical tests for the adequacy of the simulations, such as χ^2, but this is beyond the scope of the present discussion.

4. Results and analysis examples

In the following we present analyses and discuss results for several materials where accurate predictions are important for the design and planning of future fusion experiments and power plants.

4.1. Nickel

Nickel is an important material in both the fusion and fission industries. It is a primary constituent of austenitic stainless steels such as 316-grade (12.5 wt.% Ni), which is the main steel proposed for the vacuum containment vessel of future fusion power plants [5]. Nickel also forms the majority of high-nickel Inconel super-alloys such as 718-grade (nominal Ni content 52.44 wt.%), which are oxidation-corrosion-resistant materials specifically designed to function at high temperatures such as in power-generating turbines [36]. For these reasons, the cross sections of nuclear reactions on nickel isotopes are well-studied (see, for example [37–39]). However, with five naturally occurring stable isotopes (^{58}Ni 68.077 atm.%, ^{60}Ni 26.223%, ^{61}Ni 1.140%, ^{62}Ni 3.635%, and ^{64}Ni 0.926%) the nuclear reaction landscape for nickel is very complex. Fortunately, the detailed FISPACT-II simulations performed for the FNS benchmark and the in-depth interpretation analysis afforded by them, allow this complexity to be understood.

Figure 2 displays the main graphical outputs from the simulated experiment on nickel. The top plots (figures 2(*a*) and (*b*), for the 5 min and 7 h experiments, respectively) show total decay-heat evolution curves from FISPACT-II simulations with the five different nuclear libraries [30–33, 35] alongside the experimental measurement points (with the small experimental uncertainties as vertical lines)—all in μW g^{-1}. The plots also show the nuclear-data-derived uncertainty bands, which are propagated directly from the Monte Carlo-based uncertainty data included with the TENDL-2017 [30] library (see [40] for more details).

In figures 2(*c*) and (*d*) the TENDL-2017 simulations are broken-down into individual radionuclide contributions (and also compared against the experiment). Uniquely, FISPACT-II automatically formats the inventory data into output that can be used to produce these very instructive, radionuclide-separated plots directly (i.e. without any additional processing),

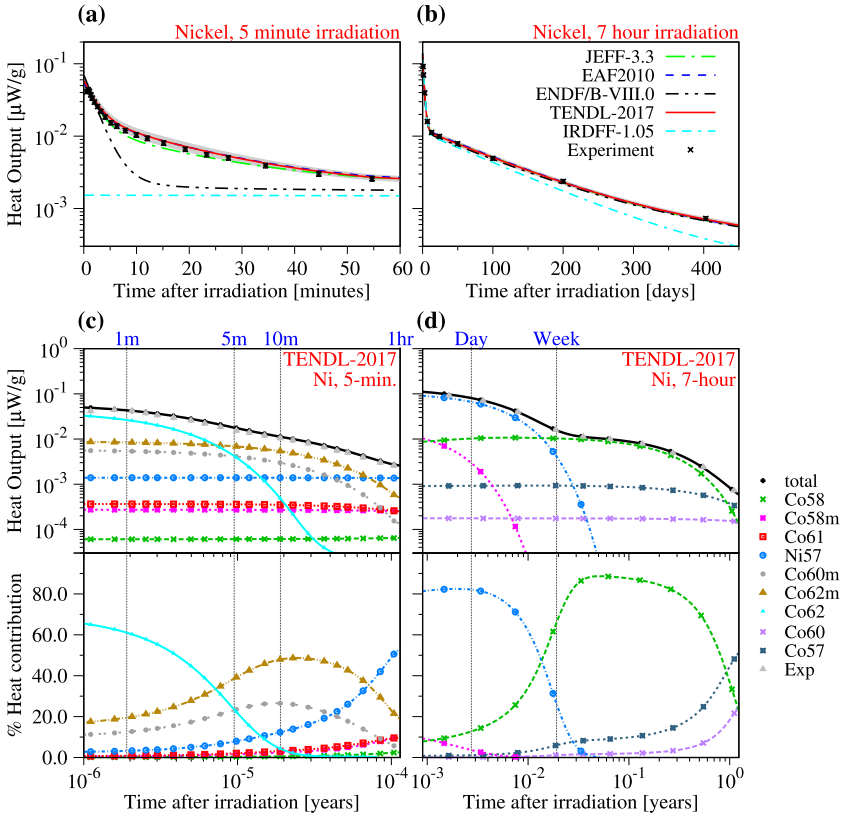

Figure 2. Simulated decay-heat experiment for nickel in the FNS benchmark. (*a*) and (*c*) Correspond to decay-heat following 5 min irradiations, (*b*) and (*d*) are the equivalent data after 7 h irradiations. (*a*) and (*b*) Show total decay-heat curves on linear time-after-irradiation scales for the different nuclear library simulations with FISPACT-II, the experimental measurements as points with vertical lines showing experimental uncertainty, and the nuclear-data-uncertainty band (in grey) for the TENDL-2017 [30] library. (*c*) and (*d*) Present the radionuclide breakdown of contributions to the total decay-heat from the TENDL-2017 simulations in absolute μW g^{-1} terms (top halves) and as % contributions (bottom halves)—on logarithmic time-after-irradiation scales. See main text for more details.

and even produces the necessary scripts for immediate use with the Gnuplot [41] plotting software (see [11] for examples and details). The authors have demonstrated previously how these plots allow straightforward understanding of complex inventory simulations [5, 42], and such plots are often used to interpret fusion inventory simulations (see, for example [43–45]).

Here, these absolute decay-heat contribute plots (top halves of figures 2(*c*) and (*d*)) are accompanied by a new variant—where the nuclide contributions are plotted as % relative contributions to the total decay-heat (lower-halves of figures 2(*c*) and (*d*)). These have recently been prototyped as part of the FNS benchmark to simplify visual identification of the important radionuclides in complex cases where there are many minor contributions, such as depicted here for nickel. Relative ratio plots may be unfamiliar in fusion research, but similar, relative/fractional contribution techniques have been applied in fission core fuel burn-up and spent nuclear-fuel analysis (e.g. [46–48]).

The nickel results show that the majority of the nuclear libraries considered produce total simulated decay-heat evolution that agrees well with the experimental measurement. The experimental values are, on average, within 10% of the simulated values for TENDL-2017, EAF2010, and JEFF-3.3 for the 5 min experiment (i.e. experiment-over-calculation or E/C ratios nominally lie in the range 0.9–1.1). This is a good result for the simulations given the short-lived and exotic nature of the radionuclides shown to be involved. The lower plot in figure 2(*c*) shows that the first 5 min of the post-irradiation cooling is dominated by ^{62}Co, whose production levels all of the general purpose libraries (i.e. excluding IRDFF-1.05) agree upon. This is an interesting observation given that it is produced almost entirely via (n,p) reactions on ^{62}Ni, which makes up only 3.6 atomic % of pure nickel—as shown in table 1, which summarises the production pathways for the important radionuclides discussed in this paper. The fact that the decay-heat can be dominated by a radionuclide whose parental-source is a relatively minor component of the starting composition demonstrates that radiological analysis must often be concerned with minor components of the overall transmutation picture (see also [49], where it is shown that very minor compositional impurities can lead to problems with predicted waste disposal).

Beyond 5 min of cooling two metastable nuclides of cobalt—^{60m}Co and ^{62m}Co—dominate for the next 30 min of experimental measurement time. Here the major nuclear libraries differ. ENDF/B-VIII.0 lacks the production pathways (both (n,p) reactions, see table 1) for these metastable isomers, while the good agreement to the experiment for the other libraries strongly suggests that these are the correctly identified sources of the measured decay-heat. Meanwhile, the IRDFF-1.05 library is not concerned with such short-lived

Table 1. List of contributing reaction-route pathways for the important radionuclides identified in the material cases discussed in the main text. Full pathway analyses for each experimental simulation can be found in the main benchmark report [21]. These pathways were identified using the tree-search algorithm employed in FISPACT-II, via the UNCERT and LOOKAHEAD keywords—see [12] for more details. IT stands for isomeric transition.

Product	$T_{1/2}$	Relevant experiment	Pathways	Path % TENDL-2017
^{62}Co	1.50 min.	Ni, 5 min.	^{62}Ni(n,p)^{62}Co	98.7
^{60m}Co	10.47 min.	Ni, 5 min.	^{60}Ni(n,p)^{60m}Co	99.4
^{62m}Co	13.91 min.	Ni, 5 min.	^{62}Ni(n,p)^{62m}Co	100.0
^{57}Ni	1.50 d	Ni, 5 min.& 7 h	^{58}Ni(n,2n)^{57}Ni	100.0
^{58}Co	70.87 d	Ni, 7 h	^{58}Ni(n,p)^{58}Co	80.0
			^{58}Ni(n,p)^{58m}Co(IT)^{58}Co	20.0
^{57}Co	271.77 d	Ni, 7 h	^{58}Ni(n,np)^{57}Co	97.1
^{56}Mn	2.58 h	Fe, 5 min. & 7 h	^{56}Fe(n,p)^{56}Mn	98.6 (in 7 h case)
^{54}Mn	312.16 d	Fe, 7 h	^{54}Fe(n,p)^{54}Mn	100.0
^{90}Y	2.67 d	Nb, 7 h	^{93}Nb(n,α)^{90}Y	69.3
			^{93}Nb(n,α)^{90m}Y(IT)^{90}Y	31.1
^{92m}Nb	10.15 d	Nb, 7 h	^{93}Nb(n,2n)^{92m}Nb	100.0
^{185m}W	1.67 min.	W, 5 min.	^{186}W(n,2n)^{185m}W	98.2
^{185}W	75.12 d	W, 5 min. & 7 h	^{186}W(n,2n)^{185}W	59.8[a]
			^{186}W(n,2n)^{185m}W(IT)^{185}W	40.0[a]
^{186}Ta	10.5 min.	W, 5 min.	^{186}W(n,p)^{186}Ta	100.0
^{187}W	23.85 h	W, 5 min.	^{186}W(n,γ)^{187}W	100.0
^{181}W	120.99 d	W, 7 h	^{182}W(n,2n)^{181}W	99.8
^{52}V	3.74 min.	Cr, 5 min.	^{52}Cr(n,p)^{52}V	97.7
^{51}Cr	27.70 d	Cr, 7 h	^{52}Cr(n,2n)^{51}Cr	100.0
^{190}Re	3.1 min.	Os, 5 min.	^{190}Os(n,p)^{190}Re	100.0
^{189m}Os	5.81 h	Os, 5 min	^{190}Os(n,2n)^{189m}Os	92.7
^{191m}Os	13.1 h	Os, 5 min.	^{192}Os(n,2n)^{191m}Os	99.1
^{190m}Os[b]	9.9 min.	Os, 5 min.	^{190}Os(n,n′)^{190m}Os	94.8 (EAF2010)

[a] Path % for production of ^{185}W during a 7 h irradiation. In the shorter, 5 min irradiation case the single-step direct reaction to route ^{185}W is higher contributor at 71.6% because the half-life of ^{185m}W is of a similar magnitude to the irradiation time.
[b] Radionuclide ^{190m}Os is only produced in simulations with EAF2010.

radionuclides, and thus, for the 5 min experiment, only predicts the low-level decay-heat from the longer-lived (and thus important for dosimetry) ^{57}Ni and ^{58}Co radionuclides (which are important for the 7 h experiment, see below).

Note for the 5 min irradiation, that none of these three identified major-contributing nuclides, ^{60m}Co, ^{62m}Co, or ^{62}Co, are dominant enough at any particularly cooling time to be unequivocally validated by this integral benchmark. Even at the start of cooling, where ^{62}Co is most dominant, it still only contributes around 67% of the decay-heat and thus it is difficult to say without any doubt that the cross section for the associated (n,p) reaction is conclusively and numerically validated. All this integral benchmark can say is that the total decay-heat profile is correctly predicted and there is some confidence in the apportionment of the contributions from different radionuclides. This illustrates a common difficulty in using integral experiments to provide quantitative input to nuclear reaction data evaluations—only in rare cases is the inventory picture simple enough to make a conclusive quantitative assessment of the spectrum-averaged cross section a single reaction (for example, see the discussion of the iron experiments below) [50].

On the other hand, ^{57}Ni, which becomes the main decay-heat generator after an hour of cooling in the 5 min experiments, is dominant enough at the start of cooling following the 7 h irradiation to be more reliably validated by that experiment. The greater than 80% dominance of ^{57}Ni (figure 2(*d*)) justifies attributing characteristic E/C values and their associated uncertainties to the production of this nuclide. The E/C_{T17} ratio, where C_{T17} refers to the calculations with TENDL-2017 (T17), taken from the time =0 measurements where the nuclide is most dominant, for 'the production of ^{57}Ni from ^{58}Ni' is 0.95, with an experimental uncertainty of 5% and nuclear data uncertainty (for the (n,2n) reaction that produces ^{57}Ni—see table 1) of 13% [21]. In the benchmark report [21], a threshold of 75% dominance is used globally to make the determination as to whether a particular time-measurement pair can validate the production of one radionuclide.

Similarly, ^{58}Co dominates the decay-heat between 1 week and 200 d (0.55 years) following the 7 h irradiation, and here the TENDL-2017 E/C_{T17} (at 12 d of cooling) is exactly one, with experimental and nuclear-data (for (n,p) reactions on ^{58}Ni) uncertainties of 5 and 10%, respectively.

Overall, the simulations agree well with the 7 h experimental measurements for all four of the major general-purpose libraries. Even the IRDFF-1.05 dosimetry captures the profile associated ^{57}Ni and ^{58}Co (it covers the necessary (n,p) and (n,2n) reactions in its database), although it deviates from the other curves and the experiment at the 200 d and 400 d measurements. IRDFF-1.05 lacks the necessary (n,np) reaction channel to produce the ^{57}Co that contributes 50% of the decay-heat at 400 d. This is perhaps unexpected as ^{57}Co is a

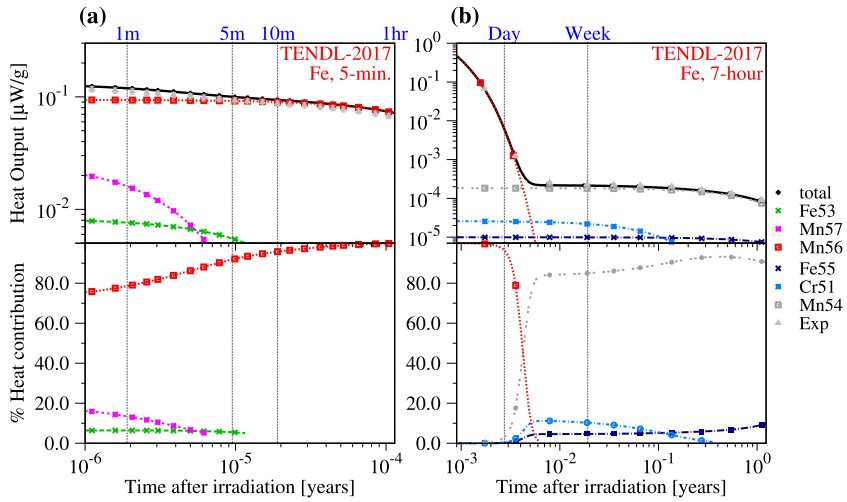

Figure 3. Radionuclide breakdown of contributions to the total decay-heat from the TENDL-2017 simulations of pure iron after (*a*) 5 min and (*b*) 7 h irradiations. Absolute μW g^{-1} curves are shown in the top halves of both plots, with % contribution-curves shown in the lower halves. The FNS benchmark experimental decay-heat measurements are also shown in the upper plots. All times are given as time-after-irradiation in years on a logarithmic scale.

γ-emitter, and is commonly used as a calibration source in nuclear medicine equipment [51] and as a radioactive marker in medicine [52], although in those cases the source of ^{57}Co is normally from cyclotron irradiation of iron, nickel, or manganese using protons [53].

4.2. Iron

Iron is perhaps even more important for fusion (and fission) than nickel, as it is the main constituent of steels, including those commonly used in the nuclear industry such as SS316 (65 wt.% Fe [5]), or those planned for future fusion application such as the reduced-activation ferritic-martensitic (RAFM) EUROFER-steel (89 wt.% Fe [5]). For this reason, the important reaction cross sections on Fe isotopes have long been studied and measured experimentally, even at 14 MeV fusion energies (see, e.g. [54–56]).

Unsurprisingly, the quality of the match between the simulations and the decay-heat experiment is very good, even allowing for some unexplained experimental variation between various batches of 5 min irradiations at the FNS facility [21]. In cooling simulations following either 5 min or 7 h irradiations, the E/C values are generally within 0.1 of one at all cooling times for all nuclear libraries considered [21]. IRDFF-1.05 shows some higher deviation due to the absence of reaction channels associated with the minor contributors to the decay-heat—see figure 3—but includes the important production routes to radionuclides of manganese that capture the majority of the decay-heat.

Figure 3 shows the absolute and % breakdown of nuclide contributions to the TENDL-2017 inventory simulation results. The picture is much simpler here than compared to nickel. In the 5 min irradiation case, one radionuclide contributes at least 70% of the total decay-heat at all cooling times, including virtually 100% beyond 10 min. This nuclide, ^{56}Mn, produced primarily via (n,p) reactions on ^{56}Fe (see table 1), also dominates at near 100% levels at the first experimental measurement time ($\sim$15 h) and during the first day of simulated cooling in the 7 h irradiation scenario. It is then replaced, in dominance, by decay-heat from ^{54}Mn (also from (n,p) reactions, this time on ^{54}Fe), which contributes at least 80% for the remainder of the 400 + d of measurement time.

The dominance of these two nuclides makes it possible to validate the spectrum-averaged cross sections of the (n,p) reactions on Fe that produce them. The TENDL-2017 simulations of the 5 min and 7 h experiments agree on an E/C$_{T17}$ value of 0.95 for (n,p) on ^{56}Fe with around 5% experimental uncertainty and 20% data uncertainty—of which the latter could be viewed as overly pessimistic (from the TENDL evaluation methodology) given the quality of the match to the measurements. Meanwhile, the simulation of cooling following a 7 h irradiation gives an E/C$_{T17}$ ratio for ^{54}Mn production via (n,p) on ^{54}Fe of 1.1 (averaged over all cooling times greater than 2 d) with 6%–10% experimental uncertainty and an 11% uncertainty on the nuclear data.

This (n,p) validation for Fe is important because these reactions also produce hydrogen (i.e. the 'p') and ^{56}Fe(n,p) in particular will be the main source of hydrogen gas production in steels inside a fusion reactor. Current predictions for a demonstration fusion power plant suggest that of the order of 500 atom parts per million (appm) hydrogen will be produced for every full-power-equivalent year of operation in pure iron, corresponding to approximately 50 appm H per dpa (displacements per atom) of damage dose [57]. Hydrogen is known to induce embrittlement in iron-based alloys [58, 59], while such H-to-dpa ratios have been shown to induce up to 5% void swelling after 50 dpa in RAFM steels in a synergistic behaviour with helium (produced at around a five-times slower rate than hydrogen [57]) [60], and can even cause significant void swelling in isolation [61]. It is clear that having accurate predictions of H production rates in iron (and hence steels where iron will be the major source of hydrogen in most cases) under neutron irradiation is vital for quantifying the safe operation lifetimes of nuclear fusion components.

4.3. Niobium

Niobium is widely used in steel production, particularly as a micro-alloy stabilising element [62], and appears as a minor constituent of both main steels considered for demonstration fusion reactor applications in Europe— ~ 0.01 and 0.005 wt.% of SS316 and EUROFER, respectively [5]. At these levels, the decay-heat from pure niobium may not be a significant concern, but it is nonetheless important that its radiological response profile is accurately predicted, and thus that relevant reaction cross sections in nuclear library evaluations are good. Even minor impurities can play a large role in activation and transmutation response of nuclear materials [49]. Note that niobium is a more significant component in high-temperature nickel-based alloys such as Inconel-718 (5.1 wt.% Nb), where it helps to form the γ'' strengthening phase [36].

Figure 4, shows results from the simulated 7 h irradiation followed by cooling, and compares the predictions to the experimental measurements. The total decay-heat evolution (figure 4(*a*)) in the experiment is well-captured by simulations with three of the general purpose libraries considered—a favourable result which is replicated for those same libraries in the 5 min irradiation benchmark (not shown here, but see [21]). However, simulations with the ENDF/B-VIII.0 library show poor agreement to the measurements. Similar to the situation noted with nickel, but more severely detrimental here, the cause of the discrepancy is the absence of a reaction channel to the metastable nuclide ^{92m}Nb. The nuclide contribution breakdown from the TENDL-2017 simulations in figure 4(*b*) shows that this metastable nuclide is the dominant source of decay-heat, contributing at least 90% of the heat at all measurement times. The ENDF/B-VIII.0 result, on the other hand, (figure 4(*c*)) has no contribution from this radionuclide, and instead predicts a decay-heat profile dominated by ^{90}Y. The other libraries agree with the level of ^{90}Y predicted by ENDF/B-VIII.0, but the comparison to the experiment clearly shows that this contribution is insufficient—neither the absolute level of ^{90}Y predicted nor its 2.7 d half-life reflect the measured decay profile (^{92m}Nb has a longer, 10 d half-life and this is an obvious match to the decay curve).

Note that ^{92m}Nb is important for dosimetry purposes and so the partial (n,2n) reaction channel that produces it from ^{93}Nb (table 1) is included in the official IRDFF-1.05 release (see [34]). However, formatting interpretation issues associated with the processing of the raw point-wise continuous cross section data files into the discrete group-wise structure have caused this reaction to be omitted from the files read as IRDFF-1.05. The conversion is necessary to calculate reaction rates from a neutron-energy-flux spectrum (as described in the introduction), but in this case the ground and/or total channels of this reaction are missing from the raw files which prevents the partial channel to ^{92m}Nb from being processed. On the other hand, processing issues are not the reason for absence of ^{93}Nb(n,2n)^{92m}Nb from the ENDF/B-VIII.0—the raw point-wise, ENDF-6 [63] file for ^{93}Nb from [31] simply does not contain any data to separate the (n,2n) reaction into different isomeric-state daughters.

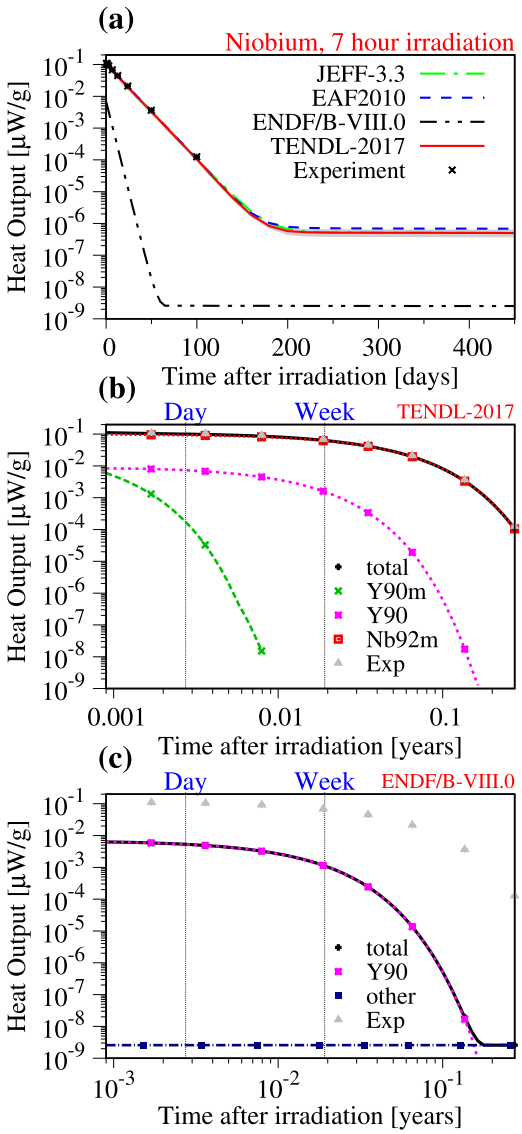

Figure 4. Simulated decay-heat experiment for a 7 h irradiation of niobium in the FNS benchmark. (*a*) Shows total decay-heat curves on a linear time-after-irradiation scale for inventory simulations with different nuclear libraries, as well as the experimental measurements as points with vertical lines showing experimental uncertainty, and the nuclear-data-uncertainty band (in grey) for the TENDL-2017 [30] library. (*b*) Presents the radionuclide breakdown of contributions to the total decay-heat from the TENDL-2017 simulation in absolute μW g^{-1} terms on a logarithmic time-after-irradiation scale. (*c*) Shows the equivalent profiles for the simulation with ENDF/B-VIII.0 [31].

The dominance of ^{92m}Nb (with three libraries at least) allows this integral experiment to more definitively validate the (n,2n) channel that produces it. The TENDL-2017 predictions give an E/C$_{T17}$ of 1.05 with 6% experimental uncertainty and a nuclear-data uncertainty (for the reaction channel) of 18%.

Validation of ^{92m}Nb production from ^{93}Nb also provides some indirect verification of the same reaction to the ground-state ^{92}Nb. This latter nuclide, with its extremely long, 3.5×10^7 year half-life is relatively difficult to measure experimentally because its radiological contribution cannot be easily measured above the dominance of its shorter-lived

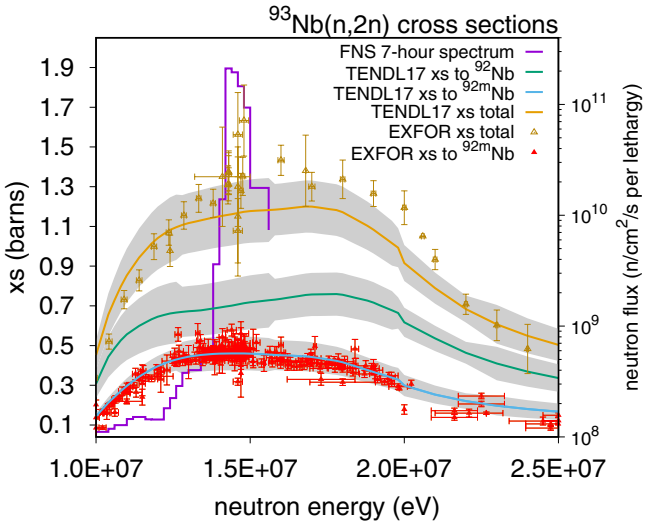

Figure 5. TENDL-2017 and EXFOR-differential cross sections for (n,2n) on ^{93}Nb. Grey uncertainty bands shown for each cross section (xs) curve are based on covariance data in the TENDL-2017 library. The TENDL-2017 total is the sum of the channels to the different daughter isomeric states (and the uncertainty band in this case comes from the individual errors summed in quadrature). EXFOR [16] data is separated into differential points (a mixture of experimental, derived, and calculated values) identified as corresponding to the metastable ^{92m}Nb or total (no EXFOR data is directly attributed to the xs of the ground-state). Quoted uncertainties in energy and xs for each differential point are shown as horizontal and vertical error-bars. The neutron energy-flux spectrum for the 7 h FNS irradiation is also shown (using the right hand *y*-axis flux scale).

isomer, and so indirect validation of this kind is useful. There is a large amount of differential EXFOR [16] data (experimental, derived, and calculated) for the production of the metastable 92*m* isomer via the ^{93}Nb(n,2n) channel, as shown in figure 5, which compares the available EXFOR data to TENDL-2017 (group-wise) cross section curves. There is also some data for the total production cross section (again, shown in the figure), but nothing for the production of ^{92}Nb. TENDL-2017 nicely captures the cross section for the production of ^{92m}Nb, particularly around the 14 MeV-peak of the FNS spectrum—nearly all of the EXFOR data points lie within the library uncertainty bands. The fact that the total ^{93}Nb(n,2n) from TENDL-2017 is also a reasonable match to the differential data in figure 5 validates the branching ratio of the reaction to the different isomers. The ratio varies between 0.3 and 0.4 in the energy range shown in the figure and is close to 0.4 at 14 MeV (i.e. 40% of the total cross section is attributed to production of ^{92m}Nb). In other words, the cross section for metastable production is approximately two-thirds of the cross section for ground-state production at 14 MeV. Thence, the validation of ^{92m}Nb creation in this integral (but largely 14 MeV) experiment also provides confidence in the ground state production.

Here it is important to note a significant omission from the niobium benchmark, which highlights a general deficiency of the (relatively) short experimental timescales. It has recently been shown [49] that ^{94}Nb production is a major concern for the waste disposal prospects of steels in a nuclear fusion demonstration power plant. This long-lived radionuclide is produced via neutron capture reactions on ^{93}Nb, which have the highest cross sections (probabilities) for occurrence at thermal energies. Such low-energy neutrons are rare in the fusion environment (including in the present FNS experiment), and so ^{94}Nb is produced slowly. However, it has a very long half-life of 20 000 years and thus does not decay significantly even on the 1000 year timescale. The FNS experimental benchmark is unable to say anything about the reaction cross sections that produce this radionuclide due to the shortness of both the irradiation (not enough ^{94}Nb is born) and cooling (insufficient time passes) times. While, the case of ^{94}Nb may be an extreme example, it is nonetheless true in general that the experimental timescales employed in Japan cannot capture all of the inventory evolution that will occur in a full fusion-reactor life-cycle. Similarly, the iron or nickel experiments do not capture ^{60}Co ($T_{1/2} = 5.3$ years) production—a nuclide also predicted to be important for limits of disposal of fusion waste.

4.4. Tungsten

Beyond structural materials (steels, etc), tungsten is probably one of the most important candidate functional materials in fusion reactor research. Significant design [3, 4, 45], experimental [64–66], and modelling effort [67–69] has been devoted to exploring how tungsten can be employed as a protective armour layer in plasma-exposed surfaces of a magnetic-confinement fusion reactor, where it is the obvious choice due to its high-melting point, low sputtering/erosion rates, and good thermal conductivity [70]. However, the predictions for activation and transmutation/burn-up of tungsten, which rely on having good quality nuclear data, are complicated and full of subtlety. For example, transmutation in W (and, to a lesser extent, its activation) can be strongly influenced by the local neutron and material environment due to self-shielding effects caused by the giant resonances in the neutron capture (n,γ) cross sections on most of tungsten's five naturally occurring isotopes [70, 71].

Figure 6 shows the full FNS benchmark result for tungsten, including 5 min (figures 6(*a*) and (*c*)) and 7 h (figures 6(*b*) and (*d*)) results. Following the 5 min irradiation, the total decay-heat profile predicted by three of the libraries considered for this case are a good match to the shape of the measurement profile. However, the decay-heat is systematically over-predicted by the inventory simulations demonstrating discrepancies in the nuclear data for this element.

The radionuclide breakdown of the TENDL-2017 simulation in figure 6(*c*) shows that the dominant radionuclide during the first 10 min of cooling after the 5 min irradiation is ^{185m}W produced by (n,2n) reactions on ^{186}W (28.43 atm.% of natural W). This radionuclide contributes almost 100% of decay-heat in the first five minutes of cooling, but the E/C$_{T17}$ during this time-frame is a very poor 0.5 with 8% nuclear data uncertainty (i.e. for the (n,2n) reaction), and a flat 13% experimental uncertainty. If the experimental measurements are to be believed then they would indicate that the

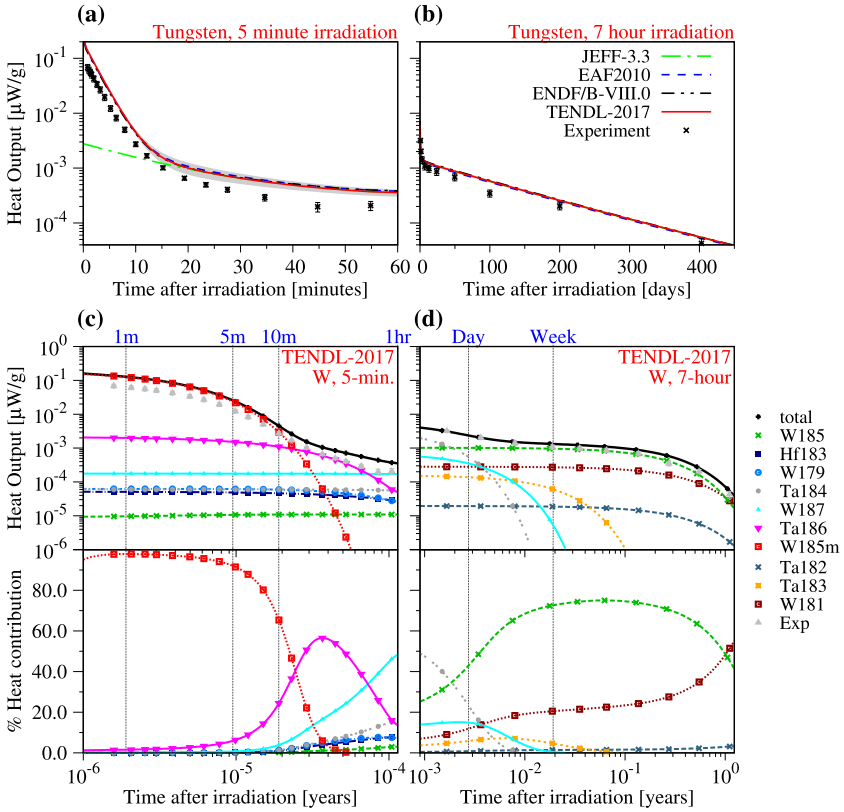

Figure 6. Simulated decay-heat experiment for tungsten in the FNS benchmark. (*a*) and (*c*) Correspond to decay-heat following 5 min irradiations, (*b*) and (*d*) are the equivalent data after 7 h irradiations. (*a*) and (*b*) Show total decay-heat curves on linear time-after-irradiation scales for the different nuclear library simulations with FISPACT-II, the experimental measurements as points with vertical lines showing experimental uncertainty, and the nuclear-data-uncertainty band (in grey) for the TENDL-2017 [30] library. (*c*) and (*d*) Present the radionuclide breakdown of contributions to the total decay-heat from the TENDL-2017 simulations in absolute μW g^{-1} terms (top halves) and as % contributions (bottom halves)—on logarithmic time-after-irradiation scales. See main text for more details.

^{186}W(n,2n)^{185m}W production channel needs to be re-evaluated slightly, particularly at 14 MeV. Analysis of the available differential data for the entire ^{186}W(n,2n) channel in EXFOR (figure 7) reveals that the current evaluated cross section for ^{185m}W in TENDL-2017 (and ENDF/B-VIII.0, EAF2010) is higher than the majority of data around 14 MeV, with EXFOR data falling largely outside of the TENDL-2017 uncertainty band (also shown in figure 7). Since the concentration of (and hence decay-heat from) ^{185m}W depends exponentially on the reaction rate ($\sigma\phi$ in equation (1)) only a small adjustment would be needed to produce a match between the simulations and experiment, which is entirely conceivable in light of figure 7. Note that the current evaluation of (n,2n)^{185m}W could be biased by the one anomalously high data point at ~15 MeV shown in the figure, and the large scatter in the total cross section points.

The need for accuracy of prediction for this (n,2n) reaction channel has particular importance because, as was shown in [71], it can contribute to almost 70% of the total Re production (^{185}W decays to ^{185}Re via β emission) in a typical fusion operational scenario where self-shielding reduces the capture reaction rates (which would dominate otherwise). The build-up of transmutant rhenium needs to be accurately quantified because it is known to alter the microstructure of W via the formation of irradiation-induced solute clustering (in the absence of irradiation Re can form solid solutions in W even at 25 atm.% concentrations [72]). Eventually, this clustering and segregation can lead to hardening and embrittlement [73, 74]. Meanwhile, the (n,2n) reactions on W isotopes in general are known to contribute almost 50% of the predicted NRT-dpa dose in tungsten under typical plasma-exposed first-wall conditions of a DEMO fusion reactor (see figure 3 in [75]). Further experiment may be needed to unequivocally prove the case for re-evaluation of these reactions (particularly on ^{186}W) for this problematic, from a nuclear data perspective, element.

For the remaining 50 min of measurement time after the 5 min irradiation, the TENDL-2017 simulation shows several contributing nuclides, with none contributing more than 50%. Interestingly, the main contributors, ^{186}Ta and ^{187}W, both originate from reactions on the same ^{186}W nuclides (see table 1). Despite other W isotopes accounting for more than 70% of all atoms in the input sample (assuming 100% purity) only ^{186}W reactions are seen to be relevant for the measured decay-heat. Since the overestimation of the experiment continues at the same factor two level (i.e. E/C $\approx$ 0.5) with all libraries (including JEFF-3.3) this could imply a more fundamental issue with ^{186}W cross sections. However, particular caution should be taken here to avoid overstating the disagreement for a capture reaction (to ^{187}W) which anyway is not strongly probed by the 14 MeV peaked neutron spectrum (figure 1), even if, as in this case, the reaction has important dosimetry applications (^{186}W(n,γ)^{187}W is included in IRDFF-1.05 [34, 35]).

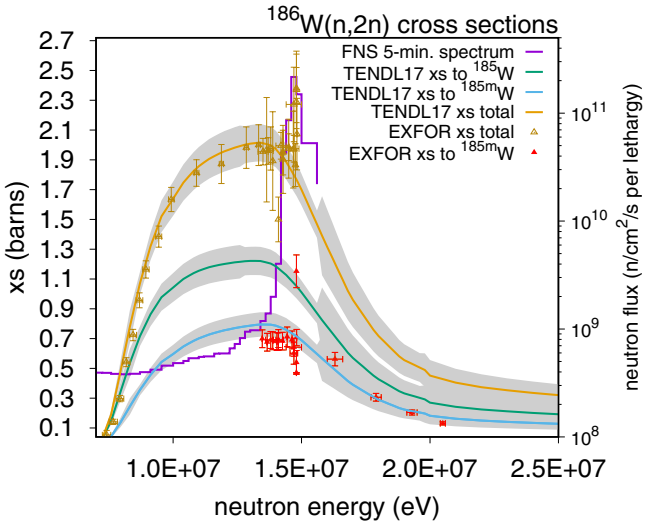

Figure 7. TENDL-2017 and EXFOR-differential cross sections for (n,2n) on ^{186}W. Grey uncertainty bands shown for each cross section (xs) curve are based on covariance data in the TENDL-2017 library. The TENDL-2017 total is the sum of the channels to the different daughter isomeric states (and the uncertainty band in this case comes from the individual errors summed in quadrature). EXFOR [16] data is separated into differential points (a mixture of experimental, derived, and calculated values) identified as corresponding to production of the metastable ^{185m}W or to the total xs. Quoted uncertainties in neutron energy and xs for each differential point are shown as horizontal and vertical error-bars. The neutron energy-flux spectrum for the 5 min FNS irradiation is also shown (using the right hand *y*-axis flux scale).

In respect of the inter-library comparison for this experiment, JEFF-3.3 [32] misses the production route to the metastable ^{185m}W nuclide and thus completely misrepresents the measured decay profile in the first 10 min following the irradiation. Meanwhile, it is not appropriate to simulate this case with IRDFF-1.05 as it is not concerned with the main radionuclides involved (in either the 5 min irradiation or the 7 h one discussed below).

Different radionuclides dominate the decay-heat during cooling in simulations of the seven-hour experiment. There are 40%–50% decay-heat contributions from ^{184}Ta and ^{181}W at the start and end, respectively, of the 400 d of cooling, but the simulated-production of neither is particularly validated by this experiment. On the other hand, the overestimation from the simulations at 403 d (the experimental measurement time) of cooling where ^{181}W is 50% of the decay-heat adds additional reason to doubt (n,2n) channel evaluations on W (^{181}W is produced via (n,2n)—see table 1).

Once again, it is the same (n,2n) channel on ^{186}W that dominates at other cooling times. This time it is the longer-lived ^{185}W ground state isomer which produces around 70% of the decay-heat between 5 and 200 d of cooling. The E/C ratios vary somewhat due to experimental fluctuations, but are typically around 0.7–0.8 for this dominant channel and for all nuclear libraries considered (including JEFF-3.3 which includes the ground-state channel). As before, this estimate is based on the total decay-heat E/C ratios, with experimental and TENDL-2017-nuclear-data uncertainties of 15% and 7%, respectively.

As with the 5 min there is an over-prediction by the 7 h simulations (see figure 6(*b*)). This disagreement between simulation and experiment is not as large as in the shorter experiment, but it nonetheless gives further cause to doubt the current cross sections evaluations for ^{186}W(n,2n) (figure 7) in all library evaluations.

4.5. Chromium

Chromium, like iron and nickel, is an important constituent of steels, including those of interest for fusion power reactors, such as SS316 (18 wt.% Cr) and RAFM EUROFER (9.5 wt.%). For this reason, the measurement of nuclear reaction cross sections has been of historical and long-term interest, resulting in many published data sets, including at 14 MeV fusion energies (e.g. [76–78]). Furthermore, as with iron, one would expect the simulation predictions to accurately reproduce decay-heat measurements for this important and well-studied element. However, this assumes that the experiments are without artifact, which has been true for the other examples from the FNS benchmark considered so far, but is not the case for chromium.

Figure 8 shows the decay-heat measurements for chromium after both 5 min (figures 8(*a*) and (*c*)) and 7 h (figures 8(*b*) and (*d*)) irradiations. Unlike the situation with the previous metals (Ni, Fe, Nb, W), where a metallic foil sample was used, it was not possible for the JAEA experimentalists to obtain stable thin-foil samples of Cr and so a metallic powder was used [26]. While it was known that this chromium powder would be likely to contain impurities of Al (up to 0.2 wt.%), Fe (up to 0.6 wt.%), and several others [22, 26], exact quantification of the impurity levels was not possible during the experimental campaign and so the simulation benchmark is performed with an assumption of 100% purity. Such an assumption has no impact on the simulations of many of the other metallic-foil-based experiments because the activated impurities do not produce a noticeable decay-heat contribution, but for Cr the simulations are not so fortunate.

The simulated total decay-heat curves after Cr irradiation (figures 8(*a*) and (*b*)) show a clear underestimation of the measured decay-heat beyond 30 min of cooling in the 5 min irradiation experiment, and during the first 4–5 d of cooling following the 7 h irradiation. As was noted by Maekawa *et al* [22, 26], the latter discrepancy could easily be accounted for by a source of ^{24}Na in the sample, which has the correct 15 h half-life to match the observed decay profile and is produced via ^{27}Al(n,α)^{24}Na (a well-established reference reaction in many γ-detector applications [28]). Similarly, the additional, unaccounted for decay-heat at the end of the measurement time following the 5 min irradiation could be due to a combined contribution from not only ^{24}Na, but also the shorter-lived ^{27}Mg and ^{56}Mn produced from (n,p) reactions on ^{27}Al and ^{56}Fe, respectively (again, these are both high-cross section, standard reference reactions [27]). A FISPACT-II & TENDL-2017 simulation with 0.2 wt.% Al and 0.6 wt.% Fe in otherwise pure Cr (as suggested above), does indeed result in a simulation prediction that is a very good match to the

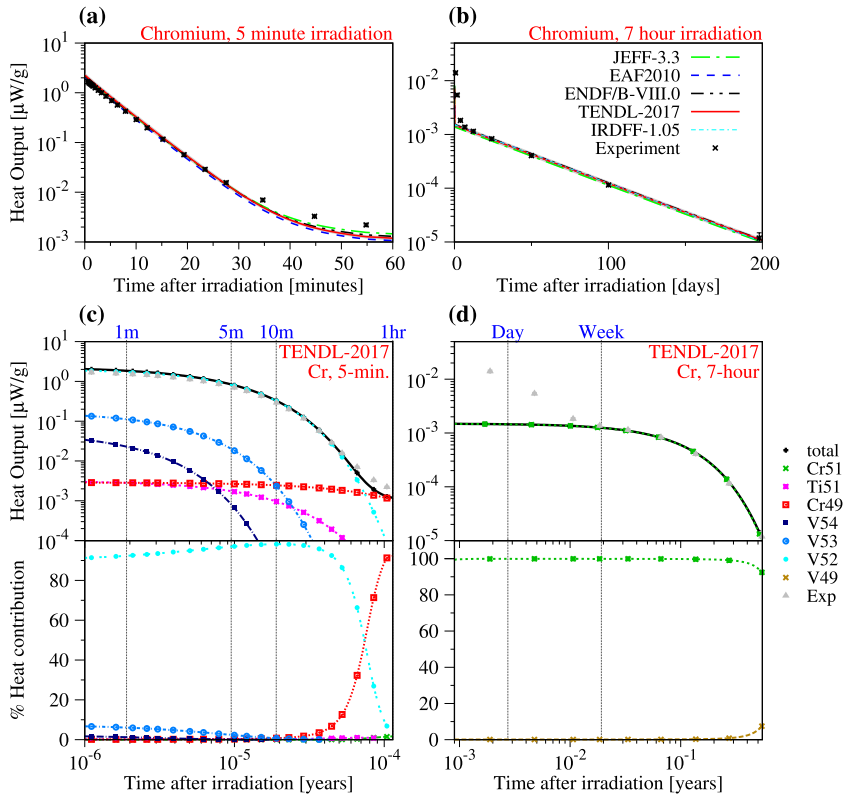

Figure 8. Simulated decay-heat experiment for chromium in the FNS benchmark. (*a*) and (*c*) Correspond to decay-heat following 5 min irradiations, (*b*) and (*d*) are the equivalent data after 7 h irradiations. (*a*) and (*b*) Show total decay-heat curves on linear time-after-irradiation scales for the different nuclear library simulations with FISPACT-II and the experimental measurements as points. Note that the experimental errors and TENDL-2017 uncertainties are plotted (as elsewhere in this paper), but are comparatively small in this case and barely visible on the plotting scales used. (*c*) and (*d*) Present the radionuclide breakdown of contributions to the total decay-heat from the TENDL-2017 simulations in absolute μW g^{-1} terms (top halves) and as % contributions (bottom halves)—on logarithmic time-after-irradiation scales. Note that the IRDFF-1.05 was not considered in simulations of the cooling after the 5 min irradiation. See main text for more details.

experimental measurements, which highlights again how important relatively minor impurities can be on measurement and simulation of radiological response.

Despite these impurity issues, the Cr experimental results are reasonably useful for integral validation purposes because the overwhelming majority of the decay-heat is predicted to come from one radionuclide in each case. For the 5 min irradiation, ^{52}V generates more than 90% of the decay-heat during the first 25 min of cooling and the simulations agree well with the measurements. The E/C values lie between 0.8 and 1.0 in this time-frame with all nuclear libraries except IRDFF-1.05, which is omitted here because the half-life of ^{52}V is too short to be of interest for dosimetry applications. The experimental error during this cooling period was 6%–8% and the TENDL-2017 uncertainty for the (n,p) reaction on ^{52}Cr that produced most of ^{52}V (see table 1) was 12%.

Similarly, in the 7 h irradiation experiment ^{51}Cr produces almost 100% of the simulated decay-heat, and, after the impurity heat has dissipated, the decay profile of this radionuclide predicted by all libraries (including IRDFF-1.05 because ^{51}Cr is important for dosimetry) closely matches the experimental measurements. E/C values are close to one for cooling times greater than one week. The low quoted experimental errors of 6%, and TENDL-2017 nuclear data uncertainty for the (n,2n) production route of 10%, allow a safe conclusion that this reaction is a good evaluation well-validated by this experiment.

4.6. Osmium

The previous results discussed in this paper demonstrated how well the often complex decay-heat simulations were able to match the experimental measurements. This final benchmark example, on the other hand, for osmium, considers a situation where inventory simulations fail to reproduce the experiment, regardless of the nuclear library choice. Like rhenium, osmium is one of the main transmutation products produced during the neutron-irradiation of tungsten in a fusion environment [70]. While concentrations of Os may never exceed 1–2 atm.% in tungsten armour, it will still be necessary to understand the radiological and transmutation response of Os as an impurity at this level. Furthermore, osmium segregates strongly in tungsten under irradiation (even more so than rhenium) [73] and can promote the formation of inter-metallic σ-phases in the ternary W–Re–Os system [70, 79], leading to hardening and embrittlement [80].

Figure 9 shows the benchmark results for the 5 min irradiation experiment on osmium. It is immediately clear from the total decay-heat curves (figure 9(*a*)) that the simulation predictions are poor for any choice of nuclear library. Even more

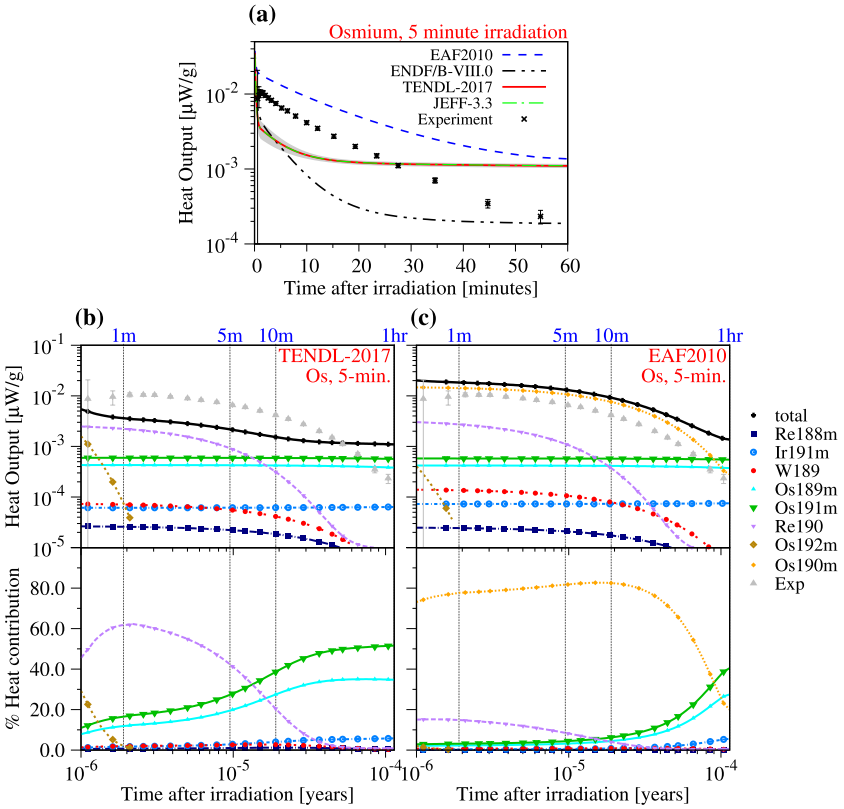

Figure 9. Simulated decay-heat experiment for a 5 min irradiation of osmium in the FNS benchmark. (*a*) Shows total decay-heat curves on a linear time-after-irradiation scale for inventory simulations with different nuclear libraries, as well as the experimental measurements as points. Vertical error lines show the experimental uncertainty and a grey band indicates the TENDL-2017 nuclear-data uncertainty. (*b*) Presents the radionuclide breakdown of contributions to the total decay-heat from the TENDL-2017 simulation in absolute μW g^{-1} terms (top half) and as % contributions (bottom half)—on logarithmic time-after-irradiation scale. (*c*) Shows the equivalent absolute and % radionuclide profiles for a FISPACT-II simulation with EAF2010 [33].

concerning is the fact that the FISPACT-II calculations with different libraries give completely different results in terms of both decay-heat values and decay-curve profile.

Firstly, notice that TENDL-2017 and JEFF-3.3 give identical results. This is not uncommon—for example, all of the other example materials discussed in this paper, where the agreement with experiments are good, have different library predictions that are often indistinguishable. However, in this case, the two libraries are identical and wrong precisely because they *are* the same. JEFF-3.3 [32] was compiled from various sources and many of its individual nuclide-target files (including both ^{190}Os and ^{192}Os, which are the main isotopes of osmium at 26.36 and 40.93 atm.%, respectively) were taken directly from the previous version of TENDL, TENDL-2015 [81]. This highlights one of the difficulties in comparing different nuclear data libraries, in particular concerning the optimal choice of library for an application—in a situation where one library differs from two (or more) others, it may not be accurate to say that library agreement points to the correct result if that agreement is produced from identical underlying data. In general, it might not be obvious that libraries are identical, unless a user is willing to analyze in-depth the origin of the cross section data for relevant nuclides.

Figures 9(*b*) and (*c*) show the nuclide decay-heat breakdown of the simulations on osmium with TENDL-2017 and EAF2010, respectively. The EAF2010 result is a significant over-prediction (E/C$_{E10}$ ratios, where E10 refers to calculations with EAF2010, range between 0.1 and 0.6 for all measurement times). However, the decay-curve profile appears to match the evolution in the experimental measurements during the first 10 min of cooling. This suggests that ^{190m}Os, with its 9.9 min half-life, which contributes at least 70% of the total decay-heat in this case, has been correctly identified as the dominant radionuclide. Indeed, looking closer at the nuclide breakdown for the EAF2010 simulation in figure 9(*c*) it appears as though the isolated ^{190m}Os decay-heat curve is actually a good match to the time-evolution for the entire one-hour measurement—its curve nicely parallels the experimental points. However, beyond 10 min of cooling, decay-heat from two longer-lived metastable isomers (^{191m}Os and ^{189m}Os) competes with ^{190m}Os, causing a deviation from the profile of that nuclide, and, as it appears, the correct experimental-measurement profile. Those latter two nuclides, whose contributions appear over-predicted, are both generated via (n,2n) reactions (see table 1) and this could be another case, as with the related W (section 4.4), where those threshold neutron-multiplication reaction channels need re-evaluating.

Meanwhile, osmium FISPACT-II simulations with TENDL-2017 (figure 9(*b*)) do not produce any ^{190m}Os. This results in a large under-prediction of the decay-heat at cooling times below 25 min and a misrepresentation of the entire measured decay-profile. In the absence of ^{190m}Os, two

separate dominant-nuclide regimes occur: below 5 min of cooling ^{190}Re contributes around 50%. Note that EAF2010 simulations also predict approximately the same absolute decay-heat values from this nuclide, but it is not relevant compared to ^{190m}Os in that simulation. TENDL-2017 also predicts nearly the same heat from ^{191m}Os and ^{189m}Os as EAF2010, and these two nuclides contribute the majority of the decay-heat for the remainder of the simulation. Once again, this produces the wrong decay profile in comparison to the experiment, and an over-prediction beyond 25 min. The ENDF/B-VIII.0 osmium simulation, on the other hand, does not predict any of ^{190m}Os, ^{191m}Os or ^{189m}Os, and so it generally under-predicts the experiment by a very wide margin.

The recommendation here, for future library releases, is that the production route for ^{190m}Os (see table 1) needs to be properly embedded in the evaluated file for ^{190}Os, although the exact scale of the cross sections, particularly around 14 MeV, needs to be carefully evaluated (i.e. in comparison to these FNS-EAF2010 simulations and EXFOR).

5. Discussion

In this paper we have described a fusion decay-heat simulation-benchmark that uses experimental measurements of decay-heat for materials irradiated in a 14 MeV fusion-neutron source. 73 different materials were measured at JAEA's FNS facility, covering pure metallic foils or powders of elements like iron and copper, complex nuclear alloys such as SS316 and Inconel-600, and oxides of elements like potassium and tin. This important experimental data-set has been available for more than 15 years but only with the latest computational advances can it now be routinely used as a standard simulation-benchmark tool for rapid assessment of the ability of nuclear data evaluations to predict fusion-reactor relevant radiological responses.

This benchmark could be used by any inventory simulator, but in this paper FISPACT-II [8] was applied to several material examples—nickel, iron, niobium, tungsten, chromium and osmium. FISPACT-II is a recently modernised and continuously upgraded code that is flexible enough to read many of the different international nuclear data libraries currently being maintained and updated around the world. As well as validating (or not) those individual libraries, performing the benchmark with multiple different libraries at the same time allows a more complete understanding. For example, no library was able to accurately predict the decay-heat from a 5 min irradiation of osmium, but the output from one of the library simulations (with EAF2010 [33]) suggested a possible route forward for producing new cross section files (for ^{190}Os) that could properly model the experiment.

An important aspect of nuclear data validation using this benchmark is how the simulation results are processed, analysed and interpreted. The integral values of, in this case, decay-heat that are directly compared to the experimental measurements are only one aspect of the often complex inventory simulation landscape. The results in this paper have exemplified how in-depth probing of the underlying complexity can allow greater insight into the reasons behind both good and poor performance against experiments.

Visualisation of nuclide contribution breakdowns, including the time-evolution in % contributions, allow easy identification of the dominant radionuclides. Extraction and plotting of this data is largely automated with FISPACT-II and the subsequent analysis of production pathways enables the experimental comparison to be attributed to the validation of specific reaction cross sections. In this paper, for example, it was shown that the 5 min irradiation of iron provided a strong validation of the 14 MeV nuclear data (in all libraries) for the (n,p) reaction on ^{56}Fe.

Interpretation of the nuclide contributions also reveals how well the simulations and input nuclear data are able to reproduce the integral measurements despite there often being competing contributions from several different radionuclides produced by very different reaction pathways. For example, most nuclear libraries, when used in FISPACT-II simulations of the 5 min irradiation of pure nickel, reproduced the experimental measurement to high accuracy, despite there being four different radionuclides (^{60}Co, ^{60m}Co, ^{62m}Co, and ^{57}Ni) that had varying, but significant, contributions during only one hour of post-irradiation cooling.

Some of the benchmark examples discussed show that nuclear data is able to capture the complex decay-heat response of materials, while others have demonstrated that there is still further improvements to be made. The results for W and Os showed that either the nuclear data for certain reactions need adjustment (re-evaluation) or that some reaction channels (pathways) to important isomeric states are completely omitted, although in this latter case the problem may be caused by the difficulties associated with meeting the specific formatting requirements of standardized reaction cross section files (i.e. the ENDF-6 [63] format used by many libraries and read by FISPACT-II).

A more detailed inter-comparison of nuclear data library performance has been discussed elsewhere [21, 57], but even in the limited examples presented in this paper we have seen some significant differences with supposedly general purpose libraries. In isolation these differences cannot be rationalized (which is correct?), but in conjunction with the experimental benchmark it is straightforward to identify the best performance, especially when using the nuclide breakdown information.

Acknowledgments

This work was funded by the RCUK Energy Programme [Grant Number EP/P012450/1]. The work was also partly carried out within the framework of the EUROfusion Consortium and received funding from the Euratom research and training programme 2014–2018 under Grant agreement No 633053. The views and opinions expressed herein do not necessarily reflect those of the European Commission. To obtain further information on the data and models underlying this paper please contact PublicationsManager@ukaea.uk.

ORCID iDs

M.R. Gilbert https://orcid.org/0000-0001-8935-1744

References

[1] Stork D. *et al* 2014 *J. Nucl. Mater.* **455** 277–91 (*Proc. of the 16th Int. Conf. on Fusion Reactor Materials*)
[2] Stork D. and Zinkle S.J. 2017 *Nucl. Fusion* **57** 092001
[3] Federici G., Biel W., Gilbert M.R., Kemp R., Taylor N.P. and Wenninger R. 2017 *Nucl. Fusion* **57** 092002
[4] Rieth M. *et al* 2013 *J. Nucl. Mater.* **432** 482–500
[5] Gilbert M.R., Eade T., Bachmann C., Fischer U. and Taylor N.P. 2017 *Nucl. Fusion* **57** 046015
[6] Gilbert M.R., Eade T., Bachmann C., Fischer U. and Taylor N.P. 2018 *Fusion Eng. Des.* **136** 42–8 (Special Issue: *Proc. of the 13th Int. Symp. on Fusion Nuclear Technology*)
[7] Gilbert M.R., Dudarev S.L., Zheng S., Packer L.W. and Sublet J.-Ch. 2012 *Nucl. Fusion* **52** 083019
[8] Sublet J.-Ch., Eastwood J.W., Morgan J.G., Gilbert M.R., Fleming M. and Arter W. 2017 *Nucl. Data Sheets* **139** 77–137
[9] Shimwell J., Kovari M., Lilley S., Zheng S., Morgan L.W.G., Packer L.W. and McMillan J. 2016 *Fusion Eng. Des.* **104** 34–9
[10] Heuer D., Merle-Lucotte E., Allibert M., Brovchenko M., Ghetta V. and Rubiolo P. 2014 *Ann. Nucl. Eng.* **64** 421–9
[11] FISPACT-II, release 4.0 2018 http://fispact.ukaea.uk
[12] Fleming M., Stainer T. and Gilbert M.R. 2018 *The FISPACT-II User Manual*, UKAEA-R(18)001, UKAEA, available from http://fispact.ukaea.uk
[13] Hindmarsh A C 1983 *ODEPACK, a Systematized Collection of ODE Solvers* (*IMACS Transactions on Scientific Computation* vol 1) ed R.S. Stepleman *et al* (Amsterdam: North-Holland) pp 55–64 (*Scientific Computing*)
[14] Radhakrishnan K. and Hindmarsh A.C. 1993 Description, use of LSODE, the Livermore solver for ordinary differential equations *LLNL Report* UCRL-ID-113855
[15] Fleming M., Sublet J.-Ch., and Kopecky J. 2018 Integro-Differential Verification and Validation, FISPACT-II & TENDL-2017 nuclear data libraries, UKAEA-R(18)004, UKAEA, available from http://fispact.ukaea.uk
[16] EXFOR: Experimental Nuclear Reaction Data, https://www-nds.iaea.org/exfor/
[17] Forrest R.A. 2011 *Energy Procedia* **7** 540–52 (Asian nuclear prospects 2010)
[18] Forrest R.A. 2006 *Fusion Eng. Des.* **81** 2143–56
[19] Fleming M. and Sublet J.-Ch. 2018 Validation of FISPACT-II decay heat and inventory predictions for fission events, UKAEA-R(18)003, UKAEA, available from http://fispact.ukaea.uk
[20] Fleming M. *et al* 2018 Maxwellian-averaged neutron-induced cross sections for kT =1 keV–100 keV, KADoNiS, TENDL-2014, ENDF/B-VII.1 and JENDL-4.0u nuclear data libraries UKAEA-R(18)005, UKAEA available from http://fispact.ukaea.uk
[21] Gilbert M.R. and Sublet J.-Ch. 2018 Fusion decay heat validation, FISPACT-II & TENDL-2017, EAF2010, ENDF/B-VIII.0, JEFF-3.3, and IRDFF-1.05 nuclear data libraries CCFE-R(18)002, UKAEA available from http://fispact.ukaea.uk
[22] Maekawa F. and Ikeda Y. 2000 *Fusion Eng. Des.* **47** 377–88
[23] Maekawa F., Kichiro S., Wada M., Ikeda Y. and Takeuchi H. 2002 *J. Nucl. Sci. Technol.* **39** 990–3
[24] Maekawa F. *et al* Data collection of fusion neutronics benchmarking experiment conducted at FNS/ JAERI, JAERI-Data/Code 98-021, JAEA 1998 www.jaea.go.jp/jaeri/
[25] Maekawa F. *et al* 1998 *Compilation of Benchmark Results for Fusion Related Nuclear Data* JAERI-Data/Code 98-024 (JAEA) www.jaea.go.jp/jaeri/
[26] Maekawa F., Wada M. and Ikeda Y. 1999 Decay Heat Experiment, Validation of calculation code systems for fusion reactor JAERI 99-055 and JAEA www.jaea.go.jp/jaeri/
[27] Gilbert M.R., Packer L.W. and Lilley S. 2014 *Nucl. Data Sheets* **119** 401–3
[28] Packer L.W., Gilbert M., Hughes S., Lilley S., Pampin R. and Sublet J.-Ch. 2012 *Fusion Eng. Des.* **87** 662–6 (*10th Int. Symp. on Fusion Nuclear Technology*)
[29] Pelowitz D.B. 2013 *MCNP6 User Manual, Version 1.* Los Alamos document number: LA-CP-13-00634, Rev. 0. Further details at http://mcnp.lanl.gov/
[30] Koning A.J. and Rochman D. 2018 TENDL-2017; Release Date: April 25 2018 . Available from https://tendl.web.psi.ch/tendl_2017/tendl2017.html
[31] Brown D. *et al* 2018 ENDF/B-VIII.0 Nuclear Data for Science and Technology (https://www-nds.iaea.org/endf) Release Date: February 2018 www.nndc.bnl.gov/endf/b8.0/
[32] JEFF team 2017 The JEFF-3.3: Evaluated Nuclear Data Library www.oecd-nea.org/dbdata/jeff/jeff33/index.html; Release Date: November 2017
[33] Sublet J.-Ch., Packer L.W., Kopecky J., Forrest R.A., Koning A.J. and Rochman D.A. 2010 The European activation file: EAF-2010 neutron-induced cross section library, CCFE-R(10)05, Available from www.ccfe.ac.uk/EASY2007.aspx
[34] 2014 See the list at https://www-nds.iaea.org/IRDFF/Table4.pdf
[35] Trkov A. *et al* 2014 International reactor dosimetry and fusion file IRDFF v.1.05; release date: 9 October 2014 available from https://www-nds.iaea.org/IRDFF/
[36] Nowotnik A. 2016 *Reference Module in Materials Science and Materials Engineering; Nickel-Based Superalloys* (New York: Elsevier) (https://doi.org/10.1016/B978-0-12-803581-8.02574-1)
[37] Semkova V., Avrigeanu V., Glodariu T., Koning A.J., Plompen A.J.M., Smith D.L. and Sudár S. 2004 *Nucl. Phys.* A **730** 255–84
[38] Taddei M.H.T, Macacini J.F., Vicente R., Marumo J.T., Sakata S.K. and Terremoto L.A.A. 2013 *Appl. Radiat. Isot.* **77** 50–5
[39] Schulc M., Košťál M., Novák E. and Czakoj T. 2018 *Appl. Radiat. Isot.* **140** 247–51
[40] Eastwood J.W., Morgan J.G. and Sublet J.-Ch. 2015 *Nucl. Data Sheets* **123** 84–91 (Special Issue on *Int. Workshop on Nuclear Data Covariances April 28–May 1, 2014, (Santa Fe, NM, USA) http://t2.lanl.gov/cw2014*)
[41] Merritt E.A. *et al* 2019 Current version of Gnuplot (5.2.6, 2019) available from www.gnuplot.info/
[42] Gilbert M.R., Fleming M. and Sublet J.-Ch. 2017 *EPJ Web Conf.* **146** 09017
[43] Fischer U., Pereslavtsev P., Möslang A. and Rieth M. 2009 *J. Nucl. Mater.* **386–8** 789–92 (Fusion reactor materials)
[44] Stankunas G., Tidikas A. and Fischer U. 2018 *Fusion Eng. Des.* **136** 617–22 (Special Issue: *Proc. of the 13th Int. Symp. on Fusion Nuclear Technology*)
[45] Ueda Y., Schmid K., Balden M., Coenen J.W., Loewenhoff Th., Ito A., Hasegawa A., Hardie C., Porton M. and Gilbert M. 2017 *Nucl. Fusion* **57** 092006
[46] Baybakov D.F., Godovykh A.V., Martynov I.S. and Nesterov V.N. 2016 *Nucl. Eng. Technol.* **2** 183–90

[47] Chiba G., Tsuji M., Narabayashi T., Ohoka Y. and Ushio T. 2015 *J. Nucl. Sci. Technol.* **52** 953–60
[48] Rudychev V.G., Azarenkov M.O., Girka I.O., Shchus O.P. and Rudychev Y.V. 2017 *Vopr. At. Nauki i Tekh.* **2** 91–6
[49] Gilbert M.R., Eade T., Rey T., Vale R., Bachmann C., Fischer U. and Taylor N.P. 2019 *Nucl. Fusion* **59** 076015
[50] Trkov A. and Capote R. 2017 On the use of integral experiments in nuclear data evaluation *Presented at the Consultants' Meeting on Integral Data in Nuclear Data Evaluation, (IAEA, Vienna 14–17 November 2017)* https://www-nds.iaea.org/index-meeting-crp/CM-IDNDE-2017/docs/Trkov2017-2.pdf
[51] Mettler F.A. and Guiberteau M.J. 2012 2—Instrumentation and quality control *Essentials of Nuclear Medicine Imaging (Sixth Edition)* 6th edn, ed F.A. Mettler *et al* (Philadelphia, PA: Saunders) pp 2–69
[52] Allisy-Roberts P. and Williams J. 2008 Chapter 8—Gamma imaging *Farr's Physics for Medical Imaging (Second Edition)* 2nd edn, ed P. Allisy-Roberts *et al* (Philadelphia, PA: Saunders) pp 121–45 https://doi.org/10.1016/B978-0-7020-2844-1.50012-0
[53] IAEA 2009 *Cyclotron Produced Radionuclides* (*Physical Characteristics and Production Methods, Series* vol 468) (Vienna: IAEA) (https://www-pub.iaea.org/MTCD/Publications/PDF/trs468_web.pdf)
[54] Kudo K., Michikawa T., Kinoshita T., Kobayashi N., Fukuda A., Hino Y. and Kawada Y. 1987 *J. Nucl. Sci. Technol.* **24** 684–92
[55] Rao Venugopala P. and Fink R.W. 1967 *Phys. Rev.* **154** 1023–8
[56] Nagel W. and Aten A.H.W 1965 *Physica* **31** 1091–5
[57] Gilbert M.R. and Sublet J.-Ch. 2017 *Fusion Eng. Des.* **125** 299–306
[58] Xu Q. and Zhang J. 2017 *Sci. Rep.* **7** 16927
[59] Dadfarnia M., Novak P., Ahn D.C., Liu J.B., Sofronis P., Johnson D.D. and Robertson I.M. 2010 *Adv. Mater.* **22** 1128–35
[60] Zinkle S.J., Boutard J.L., Hoelzer D.T., Kimura A., Lindau R., Odette G.R., Rieth M., Tan L., and Tanigawa H. 2017 *Nucl. Fusion* **57** 092005
[61] Kupriiyanova Y.E., Bryk V.V., Borodin O.V., Kalchenko A.S., Voyevodin V.N., Tolstolutskaya G.D. and Garner F.A. 2016 *J. Nucl. Mater.* **468** 264–73
[62] Deardo A.J. 2003 *Int. Mater. Rev.* **48** 371–402
[63] Herman M. *et al* 2012 *ENDF-6 Formats Manual, Data Formats and Procedures for the Evaluated Nuclear Data File ENDF/B-VI and ENDF/B-VII* volume BNL-90365-2009 Rev.2 (Brookhaven National Laboratory) https://www-nds.iaea.org/public/endf/endf-manual.pdf
[64] Khripunov B.I., Koidan V.S., Ryazanov A.I., Gureev V.M., Kornienko S.N., Latushkin S.T., Rupyshev A.S., Semenov E.V., Kulikauskas V.S. and Zatekin V.V. 2015 *Phys. Procedia* **71** 63–7 (*18th Conf. on Plasma-Surface Interactions (Moscow, Russian Federation, 5–6 February 2015) and the 1st Conf. on Plasma and Laser Research and Technologies (Moscow, Russian Federation, 18–20 February 2015)*)
[65] Krupin V.A. *et al* 2017 *Nucl. Fusion* **57** 066041
[66] Klimenkov M., Jäntsch U., Rieth M., Schneider H.C., Armstrong D.E.J., Gibson J. and Roberts S.G. 2016 *Nucl. Mater. Eng.* **9** 480–3
[67] Marian J. *et al* 2017 *Nucl. Fusion* **57** 092008
[68] Wróbel J.S., Nguyen-Manh D., Kurzydłowski K.J. and Dudarev S.L. 2017 *J. Phys.: Condens. Matter* **29** 145403
[69] Sand A.E., Byggmästar J., Zitting A. and Nordlund K. 2018 *J. Nucl. Mater.* **511** 64–74 (Special Section on *18th Int. Conf. on Fusion Reactor Materials*)
[70] Gilbert M.R. and Sublet J.-Ch. 2011 *Nucl. Fusion* **51** 043005
[71] Gilbert M.R., Sublet J.-Ch. and Dudarev S.L. 2017 *Nucl. Fusion* **57** 044002
[72] Klopp W.D. 1975 *J. Less Common Met.* **42** 261–78
[73] Xu A., Beck C., Armstrong D.E.J., Rajan K., Smith G.D.W., Bagot P.A.J. and Roberts S.G. 2015 *Acta Mater.* **87** 121–7
[74] Xu A., Armstrong D.E.J., Beck C., Moody M.P., Smith G.D.W., Bagot P.A.J. and Roberts S.G. 2017 *Acta Mater.* **124** 71–8
[75] Gilbert M.R. and Sublet J.-Ch. 2018 *J. Nucl. Mater.* **504** 101–8
[76] Husain L. and Kuroda P.K. 1967 *J. Inorg. Nucl. Chem.* **29** 2665–9
[77] Holmberg P., Rieppo R., Keinänen J.K. and Valkonen M. 1974 *J. Inorg. Nucl. Chem.* **36** 715–7
[78] Ghorai S.K., Williams J.R. and Alford W.L. 1987 *J. Phys. G: Nucl. Phys.* **13** 405–10
[79] Abernethy R.G. 2017 *Mater. Sci. Technol.* **33** 388–99
[80] You Y.W., Kong X.S., Wu X., Liu C.S., Fang Q.F., Chen J.L. and Luo G.N. 2017 *Nucl. Fusion* **57** 086006
[81] Koning A.J. *et al* 2016 TENDL-2015; Release Date: January 18. Available from https://tendl.web.psi.ch/tendl_2015/tendl2015.html